

Constraining the stochastic gravitational wave background using the future lunar seismometers

Han Yan^{1,2}, Xian Chen^{1,2,*}, Jinhai Zhang³, Fan Zhang^{4,5}, Lijing Shao², and Mengyao Wang⁵

¹*Department of Astronomy, School of Physics, Peking University, 100871 Beijing, China*

²*Kavli Institute for Astronomy and Astrophysics at Peking University, 100871 Beijing, China*

³*Institute of Geology and Geophysics, Chinese Academy of Sciences, Beijing 100029, China*

⁴*Institute for Frontiers in Astronomy and Astrophysics,
Beijing Normal University, Beijing 102206, China and*

⁵*Department of Astronomy, Beijing Normal University, Beijing 100875, China*

(Dated: May 22, 2024)

Motivated by the old idea of using the moon as a resonant gravitational-wave (GW) detector, as well as the recent updates in modeling the lunar response to GWs, we re-evaluate the feasibility of using a network of lunar seismometers to constrain the stochastic GW background (SGWB). In particular, using the updated model of the lunar response, we derive the pattern functions for the two polarizations of GW. With these pattern functions, we further calculate the overlap reduction functions for a network of lunar seismometers, where we have relaxed the conventional assumption that lunar seismometers are perfectly leveled to measure only the vertical acceleration. We apply our calculation to two future lunar projects, namely, Chang'e and the Lunar Gravitational-Wave Antenna (LGWA). We find that the two projects could constrain the SGWB to a level of $\Omega_{\text{GW}}^{\text{Chang'e}} < 79$ and $\Omega_{\text{GW}}^{\text{LGWA}} < 6.7 \times 10^{-11}$, respectively. These results are better than the constraints placed previously on the SGWB in the mid-frequency band (around $10^{-3} - 10$ Hz) by various types of experiments.

I. INTRODUCTION

The idea of using the earth or the moon as a resonant gravitational-wave (GW) detector is an old one [1–3]. Early estimations suggest that the moon might be sensitive to GW at the frequencies higher than 1 milli-Hertz (mHz) [4], due to its fundamental quadrupole mode. Meanwhile, detailed theory about the seismic response to GW gradually developed from 1960s to 1980s [2, 5]. The sensitivity in such a mid-frequency band (around $10^{-3} - 10$ Hz) is a good complement to the current ground-based GW detectors like LIGO/Virgo/KAGRA [6–8], which are tuned to detect the GWs in the audible band ($10 - 10^3$ Hz). It is also complementary to the future space-borne interferometers such as LISA [9], TianQin [10] and Taiji [11], which are sensitive to mHz GWs.

Among the various signals in the mid-frequency band [12], stochastic GW background (SGWB) is a persistent one [13]. Such a background could form during the early cosmic inflation [14–16] or due to the evolution of a population of binaries in the Milky Way [17–19]. In the most optimistic scenarios, the predicted energy density from these sources amounts to $\Omega_{\text{GW}} \simeq 10^{-8} \sim 10^{-10}$ in the mid-frequency region.

Several earlier works tried to constrain the SGWB in the mid-frequency band by analyzing the data from the seismometer networks on the earth or the moon. They studied both the free-surface effect [20] (hereafter CH14a) and the normal modes [21] (hereafter CH14b) of the

earth, as well as the normal modes of the moon [22] (hereafter CH14c). However, limited by the sensitivities of the seismometers, the results are insufficient to put stringent constraint on the SGWB, even though they are already better than (or at least comparable to) the constraints placed by other types of experiments, such as ULYSSES [23], LP [24], GPS [25], GRACE-FO [26], and Tianwen-I [27]. Therefore, different designs of lunar seismometers that are underway can boost the sensitivity in this band, such as the Lunar Gravitational-Wave Antenna (LGWA) [28] and other designs (e.g., [29]).

Three recent progresses motivated us to revisit the calculation of the sensitivity of lunar seismometers to the SGWB. First, the physical interpretation and theoretical formulation of the lunar response to GW have evolved in recent years [30–32], and the response functions of the moon have been updated [31, 33, 34]. Conventionally, the lunar response to GW has been understood in two different ways, either from the tidal acceleration or from the local shear force induced by GW (the latter one corresponds to the result of an effective-field-theory approach [32]). In light of the recent studies, it becomes clear that the latter approach results in a response function which is directly proportional to the readout of a lunar seismometer. Second, deployment of new seismometers on the moon is imminent, including China's Chang'e 7 and 8 projects [35–37] which are scheduled in 2026 and 2028, and NASA's Farside Seismic Suite (FSS) scheduled in 2026 [38]. The India's Chandrayan-3 project launched in 2023 also includes the Instrument for Lunar Seismic Activity (ILSA) [39]. Understanding their sensitivity to the SGWB is urgent. Third, depending on the design of seismometer and the deployment mechanism, future lunar seismometers may not be perfectly leveled, and one

* Corresponding author.
xian.chen@pku.edu.cn

seismometer may be able to measure the accelerations in multiple directions, but the previous works commonly assumed that the seismometer arrays are responding only to the vertical acceleration. A related matter is that seismometers with different orientations are sensitive to different polarization states of the incoming GWs. But the previous works are mostly based on a single polarization state. Here, we aim to address the above issues.

The paper is organized as follows. In Section II, we review the method of calculating the lunar response to GW, and the theory of detecting the SGWB using multiple detectors. In Section III, we calculate the overlap reduction function (ORF) of lunar-seismometer array, paying special attention to the configuration in which seismometers point to arbitrary directions. In Section IV, we apply our theoretical framework to two future projects, namely, Chang'e and LGWA, to evaluate their abilities in constraining the SGWB. Finally, in Section V, we summarize our results and discuss possible aspects for future research. Throughout the paper we will adopt the International System of Units and the Minkowski metric $\eta_{\mu\nu} = \text{diag}(-1, 1, 1, 1)$, unless mentioned otherwise.

II. BASIC THEORY

In this section, we first review the surface response solution of a radially heterogeneous elastic sphere (which is a good first-step approximation to the real case of the moon) to linearly-polarized GWs, basically following [30] (hereafter Ma19) and [31] (hereafter Yan24). We also generalize this solution to account for GWs with arbitrary polarization states. Based on this solution we derive two pattern functions corresponding to the two polarizations of GW. Next, we briefly describe the calculation of the signal-to-noise ratio (SNR) of SGWB for an array of GW detectors, which introduces an ORF. Using this SNR, we evaluate the capability of using lunar seismometers to constrain the SGWB.

A. Surface response of the moon

As we have clarified in Yan24, given a linearly polarized GW,

$$\begin{aligned} \mathbf{h} &= \Re \left\{ h_0 \epsilon_{ij} e^{i(\omega_g t - \vec{k}_g \cdot \vec{r})} \right\} \\ \vec{k}_g &= (0, 0, \omega_g/c) \\ \epsilon_{ij} &= \begin{bmatrix} 1 & 1 & 0 \\ 1 & -1 & 0 \\ 0 & 0 & 0 \end{bmatrix}, \end{aligned} \quad (1)$$

the surface response of a radially heterogeneous elastic sphere can be written as:

$$\begin{aligned} \vec{\xi}(\theta, \varphi, t) &= h_0 \cos(\omega_g t) \times \\ &\left[T_r \sum_m f^m \mathcal{Y}_{2m}(\theta, \varphi) \hat{e}_r \right. \\ &+ T_h \sum_m f^m \partial_\theta \mathcal{Y}_{2m}(\theta, \varphi) \hat{e}_\theta \\ &\left. + T_h \sum_m f^m \frac{\partial_\varphi \mathcal{Y}_{2m}(\theta, \varphi)}{\sin \theta} \hat{e}_\varphi \right], \end{aligned} \quad (2)$$

where we are evaluating the response at the location of $R(\sin \theta \cos \varphi, \sin \theta \sin \varphi, \cos \theta)$ (R is the lunar radius). Following the definition in Yan24, T_r and T_h are the radial and horizontal response functions at the GW frequency $\omega_g/2\pi$. They are independent of the location of a detector or the propagation direction of GW. \mathcal{Y}_{2m} is the real spherical harmonics, and f^m is a function depending on the direction of the propagation of GW. The definitions of three base vectors in spherical coordinates are respectively

$$\begin{aligned} \hat{e}_r &= (\sin \theta \cos \varphi, \sin \theta \sin \varphi, \cos \theta), \\ \hat{e}_\theta &= (\cos \theta \cos \varphi, \cos \theta \sin \varphi, -\sin \theta), \\ \hat{e}_\varphi &= (-\sin \varphi, \cos \varphi, 0). \end{aligned} \quad (3)$$

Notice that the tensor \mathbf{h} used above refers to a single polarization state with a single frequency. Therefore, the displacement solution, Eq. (2), although widely used in the past, applies only to a single polarization.

The displacement solution can be written into a more concise form,

$$\vec{\xi}(\theta, \varphi, t) = 2T_h \mathbf{h} \cdot \hat{e}_r + (T_r - 2T_h) (\hat{e}_r \cdot \mathbf{h} \cdot \hat{e}_r) \hat{e}_r, \quad (4)$$

by combining Eqs. (22) and (25) in Yan24. The factor 2 before T_h results from the behavior of the spherical harmonics (see Yan24 for more discussions). The advantage of using the latter form is that it unifies the solutions to different polarizations. The proof is given in the Appendix. Thus, when considering a more general GW tensor:

$$\mathbf{h} = (h_+ \mathbf{e}_+ + h_\times \mathbf{e}_\times) e^{i\omega_g t}, \quad (5)$$

we can write the surface response detected by an accelerometer along the direction \hat{e}_{det} as

$$\xi = \vec{\xi}(\theta, \varphi, t) \cdot \hat{e}_{\text{det}} = (F_+ h_+ + F_\times h_\times) e^{i\omega_g t}, \quad (6)$$

in which the two pattern functions are

$$\begin{aligned} F_+ &= 2T_h (\hat{e}_{\text{det}} \cdot \mathbf{e}_+ \cdot \hat{e}_r) \\ &\quad + (T_r - 2T_h) (\hat{e}_r \cdot \mathbf{e}_+ \cdot \hat{e}_r) \hat{e}_r \cdot \hat{e}_{\text{det}} \\ F_\times &= 2T_h (\hat{e}_{\text{det}} \cdot \mathbf{e}_\times \cdot \hat{e}_r) \\ &\quad + (T_r - 2T_h) (\hat{e}_r \cdot \mathbf{e}_\times \cdot \hat{e}_r) \hat{e}_r \cdot \hat{e}_{\text{det}}. \end{aligned} \quad (7)$$

For example, if all accelerometers measure the vertical acceleration, we can set $\hat{e}_{\text{det}} = \hat{e}_r$ and the pattern functions become

$$F_A^{\text{CH14c}} = T_r (\hat{e}_r \cdot \mathbf{e}_A \cdot \hat{e}_r), \quad A = +, \times. \quad (8)$$

These functions recover the results given in CH14c.

B. Theory of detecting SGWB

For two detectors that have uncorrelated noise but have the same noise spectral density $S_n(f)$, given a SGWB with a dimensionless energy spectral density $\Omega_{\text{GW}}(f)$, the SNR in the mid-frequency region is [40]:

$$\text{SNR} = \frac{3H_0^2}{4\pi^2} \left[2T \int_{10^{-3} \text{ Hz}}^{10 \text{ Hz}} df \Gamma^2(f) \frac{\Omega_{\text{GW}}^2(f)}{f^6 S_n^2(f)} \right]^{1/2}, \quad (9)$$

where T is the observational period, and H_0 is the Hubble parameter. In the above equation, the ORF $\Gamma(f)$ for two detectors (marked with subscript 1 and 2) is defined as:

$$\Gamma(f) = \int \frac{d^2 \hat{n}}{4\pi} \int \frac{d\psi}{2\pi} \times \left[\sum_A F_1^A(\hat{n}) F_2^A(\hat{n}) \exp \left\{ i2\pi f \hat{n} \cdot \frac{\Delta \vec{x}}{c} \right\} \right] \quad (10)$$

where \hat{n} is an unit vector along the GW wave vector, ψ is the polarization angle, $A = +, \times$ represent different polarization states, and $\Delta \vec{x}$ is the separation between two detectors. Notice that for the lunar seismometer array in the frequency range lower than 10Hz, the exponential term in Eq. (10) can be ignored, and $\Gamma(f)$ usually has the same order of magnitude as $T_{r/h}^2$.

Eq. (9) can be simplified for order-of-magnitude estimation:

$$\text{SNR} \simeq \frac{3H_0^2 \Omega_{\text{GW}}(f) \Gamma(f) \sqrt{2T\Delta f}}{4\pi^2 f^3 S_n(f)}, \quad (11)$$

where Δf is the length of the integral interval. Therefore, the threshold Ω_{GW} that is possibly detectable would be

$$\Omega_{\text{GW}} \simeq \frac{4\pi^2 f^3 S_n(f) \text{SNR}}{3H_0^2 \sqrt{2T\Delta f} \Gamma(f)}. \quad (12)$$

By setting $\Delta f \simeq f$, the above equation can be further simplified to:

$$\begin{aligned} \Omega_{\text{GW}} &\simeq \frac{\eta}{H_0^2} \frac{f^{5/2}}{\sqrt{T}} \left(\frac{\sqrt{S_n}}{T_{r/h}} \right)^2 \\ &\simeq 3.45 \times 10^{-8} \left(\frac{\eta}{10} \right) \left(\frac{H_0}{70 \text{ km s}^{-1} \text{ Mpc}^{-1}} \right)^{-2} \left(\frac{f}{1 \text{ Hz}} \right)^{-3/2} \\ &\times \left(\frac{T}{1 \text{ yr}} \right)^{-1/2} \left(\frac{f^2 \sqrt{S_n}}{10^{-15} \text{ m s}^{-2} \text{ Hz}^{-1/2}} \right)^2 \left(\frac{T_{r/h}}{10^5 \text{ m}} \right)^{-2}, \quad (13) \end{aligned}$$

in which we have applied Eq. (7). The $f^2 \sqrt{S_n}$ term approximately corresponds to the sensitivity of the seismometer, and η is a factor of order unity coming from Eq. (12). Notice that this equation generally underestimates the detectability by one or two orders of magnitude, as we will discuss in Sec. IV.

III. OVERLAP REDUCTION FUNCTION

In this section, we will calculate the ORFs using our new form of lunar response solution. We begin with the ORFs for a network of two seismometers with several special configurations. We next generalize the results to two seismometers with arbitrary configurations, and end this section with the ORFs for an array of multiple seismometers.

A. The ORF of two seismometers with special orientations

We first calculate the ORFs for several special cases, for easier comparison with the previous results. For the configuration considered in CH14c [see Eq. (8)], where the seismometers are all vertical, we can calculate the ORF with

$$\begin{aligned} \Gamma^{\text{ver-ver}} &= \int \frac{d^2 \hat{n}}{4\pi} \int \frac{d\psi}{2\pi} \sum_A F_1^{A, \text{CH14c}}(\hat{n}) F_2^{A, \text{CH14c}}(\hat{n}) \\ &= T_r^2 \int \frac{d^2 \hat{n}}{4\pi} \int \frac{d\psi}{2\pi} \sum_A (\hat{e}_{r1} \cdot \mathbf{e}_A \cdot \hat{e}_{r1}) (\hat{e}_{r2} \cdot \mathbf{e}_A \cdot \hat{e}_{r2}) \\ &= \frac{2}{15} T_r^2 (1 + 3 \cos 2\delta). \quad (14) \end{aligned}$$

Here we have set $\hat{e}_{r1} = (0, 0, 1)$ and $\hat{e}_{r2} = (\sin \delta, 0, \cos \delta)$, in which δ is the angle subtended between the two seismometers by the great circle. Notice that in the low-frequency approximation the ORF does not depend on frequency. The maximum of ORF occurs when $\delta = 0$ or π . Eq. (14) is consistent with CH14a and CH14c.

It is also interesting to consider two seismometers with horizontal accelerometers (i.e., $\hat{e}_{\text{det}} \cdot \hat{e}_r = 0$). The corresponding pattern functions are

$$F_A^{\text{hor}} = 2T_h (\hat{e}_{\text{det}} \cdot \mathbf{e}_A \cdot \hat{e}_r), \quad A = +, \times. \quad (15)$$

(i) If the two horizontal accelerometers are both vertical to the plane of the great circle between the two seismometers, the ORF is:

$$\Gamma^{\text{hor1-hor1}} = \pm \frac{8}{5} T_h^2 \cos \delta, \quad (16)$$

where \pm represents two cases in which the the two accelerometers point in the same or the opposite directions, respectively. The maximum response occurs at $\delta = 0, \pi$.

(ii) If the two accelerometers are both tangent to a same great circle, the ORF is:

$$\Gamma^{\text{hor2-hor2}} = \pm \frac{8}{5} T_h^2 \cos 2\delta, \quad (17)$$

where \pm represents the cases in which the two accelerometers point in the same or the opposite *arc* directions along the great circle. The maximum value occurs when $\delta = 0, \pi/2, \pi$.

We also consider other interesting cases in which the two seismometers have different orientations. For example, if one accelerometer is vertical and another is horizontal (relative to the surface of the moon), there are two kinds of combinations depending on the direction of the horizontal detector. Using the same notations ‘ver’, ‘hor1’, and ‘hor2’ as before, we calculate the ORFs and derive

$$\Gamma^{\text{ver-hor1}} = 0, \quad (18)$$

$$\Gamma^{\text{ver-hor2}} = \mp \frac{4}{5} T_r T_h \sin 2\delta, \quad (19)$$

where \mp corresponds to the cases in which the horizontal accelerometer aligned with the great circle is pointing in or opposite to the direction of the vertical detector. The maximum response occurs when $\delta = \pi/4, 3\pi/4$.

Now there is one kind of configuration that is still missing, in which the ORF is calculated as

$$\Gamma^{\text{hor1-hor2}} = 0. \quad (20)$$

By reviewing the above results, we find that in the configurations of ‘ver-hor1’ and ‘hor1-hor2’, the ORFs are always zero. These results are due to the cancellation of the response after the integration over the 4π solid angle and 2π polarization angle.

B. The ORF of an array of seismometers with arbitrary orientations

For two seismometers with arbitrary orientations, we can calculate the ORF according to the linear dependence of the pattern function F_A on the orientation \hat{e}_{det} of the accelerometers inside the seismometers. For example, consider two seismometers placed at the same position as described in Sec. III A. We can rename the base vectors of the orientations of the two accelerometers as follows:

$$\begin{aligned} \hat{e}_{a1} &= (0, 0, 1) \\ \hat{e}_{b1} &= (0, 1, 0) \\ \hat{e}_{c1} &= (1, 0, 0) \\ \hat{e}_{a2} &= (\sin \delta, 0, \cos \delta) \\ \hat{e}_{b2} &= (0, 1, 0) \\ \hat{e}_{c2} &= (\cos \delta, 0, -\sin \delta), \end{aligned} \quad (21)$$

where a, b, c denote ‘ver’, ‘hor1’ and ‘hor2’ respectively. Noticing that the orientation vectors can be decomposed as

$$\begin{aligned} \hat{e}_{\text{det},i} &= A_i \hat{e}_{ai} + B_i \hat{e}_{bi} + C_i \hat{e}_{ci}, \quad i = 1, 2 \\ A_i^2 + B_i^2 + C_i^2 &= 1, \end{aligned} \quad (22)$$

we can write down the total ORF as

$$\begin{aligned} \Gamma &= \frac{2}{15} \times [A_1 A_2 T_r^2 (1 + 3 \cos 2\delta) \\ &\quad + 12 B_1 B_2 T_h^2 \cos \delta \\ &\quad + 12 C_1 C_2 T_h^2 \cos 2\delta \\ &\quad + 6 (A_2 C_1 - A_1 C_2) T_r T_h \sin 2\delta]. \end{aligned} \quad (23)$$

In particular, if we consider two seismometers installed nearby on the moon, which is the case of Chang’e seismometers [41] and current design of LGWA [42], we can regard δ as a small quantity. The corresponding ORF can be calculated with

$$\begin{aligned} \Gamma^{\delta \sim 0} &\simeq \frac{8}{15} T_r^2 \times \left[\sqrt{(1 - B_1^2 - C_1^2)(1 - B_2^2 - C_2^2)} \right. \\ &\quad \left. + 3(B_1 B_2 + C_1 C_2) \zeta^2 \right], \end{aligned} \quad (24)$$

where ζ is a ratio defined by $T_h = \zeta T_r$. In this specific situation the maximum value of ORF depends on r . If $\zeta^2 > 1/3$, the maximum value is $8\zeta^2 T_r^2/5$ when $B_i = C_i = 1/\sqrt{2}$, $i = 1, 2$. Otherwise, if $\zeta^2 < 1/3$, the maximum becomes $8T_r^2/15$ when $B_i = C_i = 0$, $i = 1, 2$. For two seismometers i and j that are all horizontal (i.e., $A_i = A_j = 0$), Eq. (24) can be further simplified to

$$\begin{aligned} \Gamma_{ij}^{\delta \sim 0, \text{hor}} &= \frac{8}{5} T_h^2 (B_i B_j + C_i C_j) \\ &= \frac{8}{5} T_h^2 \hat{e}_{\text{det},i} \cdot \hat{e}_{\text{det},j}. \end{aligned} \quad (25)$$

We note that these ORFs [Eq. (24) and Eq. (25)] may overestimate the SNR for the seismometer array in a small region, because two seismometers placed nearby could have gained correlated noise.

If there are more than two seismometers, the SNR for such a detector array can be calculated with the following replacement in Eq. (9) [40]:

$$T \frac{\Gamma^2(f)}{S_n^2(f)} \rightarrow \sum_{i < j} T_{ij} \frac{\Gamma_{ij}^2(f)}{S_{n,i}(f) S_{n,j}(f)}, \quad (26)$$

where the summation is taken within different pairs (i -th and j -th seismometer) of seismometers, and T_{ij} is the common operation time for each pair. If all the operational periods T_{ij} are equal, and all the noise spectrum $S_{n,i}(f)$ are the same, we can calculate the SNR by defining an ORF of the multiple-seismometer array, which reads

$$\Gamma^{\text{array}} = \sqrt{\sum_{i < j} \Gamma_{ij}^2}. \quad (27)$$

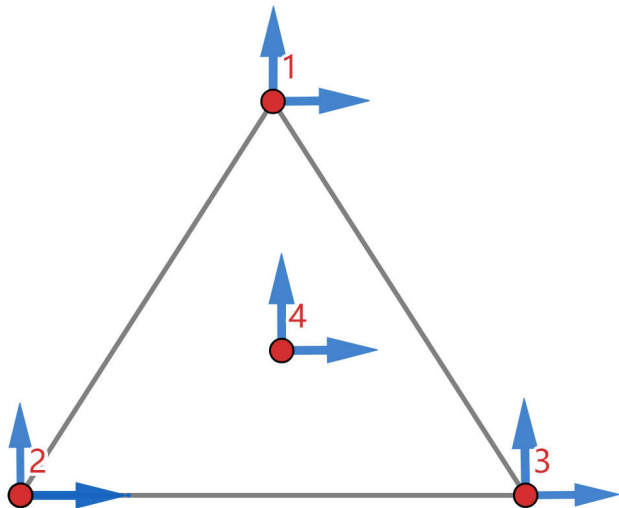


FIG. 1. Schematic diagram for the locations and orientations of LGWA seismometers. Short arrows remark the horizontal readout directions. The distances between these seismometers are around several kilometers, much smaller than the radius of the moon.

For example, for two seismometers in Chang’e 7 and 8 projects, each of them might be able to simultaneously measure the seismic responses from three orthogonal directions. Therefore, the ORF for Chang’e seismometers can be estimated as follow:

$$\Gamma^{\text{Chang'e}} \simeq \frac{8}{15} \sqrt{T_r^4 + 18T_h^4}, \quad (28)$$

where we have assumed that six readout directions just correspond to the base directions defined in Eq. (21).

For LGWA, three seismometers are placed on the vertices of a small equilateral triangle (kilometer scale) and one seismometer is placed at the center of this triangle (all seismometers have two orthogonal horizontal readouts). We plot Fig. 1 as a sketch for their locations and directions (notice that we have specified the readout directions of each seismometer for simplicity, which might not be the real case). In this case, we first calculate the ORF between each pairs:

$$\Gamma_{12} = \Gamma_{13} = \Gamma_{14} = \Gamma_{23} = \Gamma_{24} = \Gamma_{34} = \frac{8}{5} \sqrt{2} T_h^2. \quad (29)$$

The $8T_h^2/5$ term in the above equation comes from $x-x$ or $y-y$ correlation in each pair of the seismometers, which can be easily calculated using Eq. (25), and the combination of these correlations leads to an extra factor of $\sqrt{2}$, according to Eq. (27). As a result, the ORF for LGWA seismometer array becomes

$$\Gamma^{\text{LGWA}} \simeq \sqrt{C_4^2} \times \frac{8}{5} \sqrt{2} T_h^2 = \frac{16\sqrt{3}}{5} T_h^2. \quad (30)$$

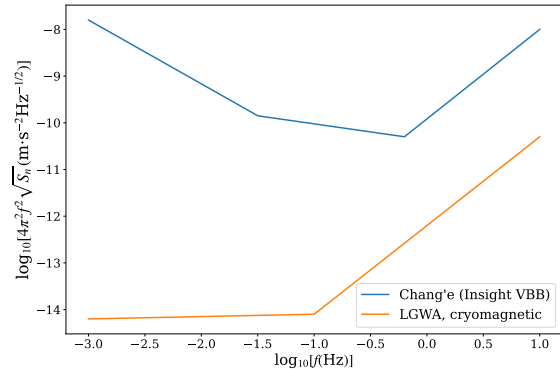


FIG. 2. The sensitivities of the seismometers in two future projects, namely Chang’e (approximated by the Insight VBB) and LGWA cryomagnetic design.

IV. CONSTRAINING THE SGWB BY LUNAR SEISMOMETERS

In this section, we will evaluate the viability of using lunar seismometers to constrain the SGWB. We mainly consider two different projects: one is the Chang’e project from China and the other is the LGWA project from Europe. We approximate the sensitivity of the seismometers of Chang’e 7 and 8 by the sensitivity of the Insight’s Very Broad Band (VBB) seismometer on Mars [43], and for LGWA we choose the cryomagnetic design [28]. The sensitivity curves of these seismometers are plotted in Fig. 2.

Next, we calculate the constraint on the energy spectral density of the SGWB by Chang’e and LGWA. According to Eqs. (28) and (30) and the related discussions in Sec. III B, we set $\Gamma^{\text{Chang'e}} = 8\sqrt{T_r^4 + 18T_h^4}/15$ and $\Gamma^{\text{LGWA}} = 16\sqrt{3}T_h^2/5$. Then the detection thresholds are derived in two different ways. (i) First, we use the approximation, Eq. (12), and set $\Delta f = f$, $\text{SNR} = 1$, and $T = 1\text{yr}$. The results are shown in Fig. 3 as the solid lines. (ii) Second, we perform a more accurate integration using Eq. (9), where we have assumed a flat spectrum for Ω_{GW} [i.e., setting $\Omega_{\text{GW}}(f) = \Omega_{\text{GW}}$], and set $\text{SNR} = 1$ and $T = 1\text{yr}$. The integration is performed in the frequency domain of $10^{-3} - 10$ Hz. The corresponding thresholds are shown in Fig. 3 as the horizontal dashed lines. The values corresponding to these two dashed lines are $\Omega_{\text{GW}}^{\text{Chang'e}} = 79$ and $\Omega_{\text{GW}}^{\text{LGWA}} = 6.7 \times 10^{-11}$, respectively. It is worth mentioning that our approach can be easily extended to the cases with different shapes of SGWB energy spectrum, by changing the constant Ω_{GW} to a certain kind of function $\Omega_{\text{GW}}(f)$ in Eq. (9). In general, the sensitivity of LGWA might enable people to distinguish the differences between different SGWB models.

For comparison, we also plot in Fig. 4 the constraints on the SGWB in the mid-frequency band given by previous works. We find that in the frequency band around

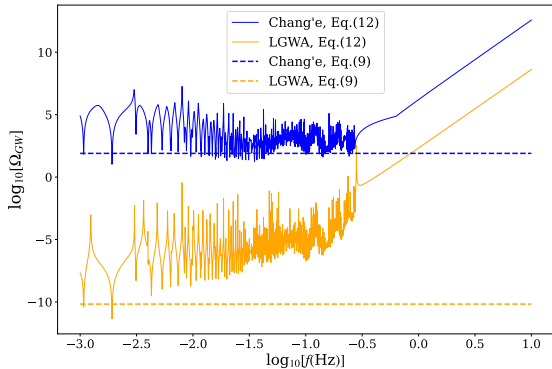


FIG. 3. Constraints on the SGWB by Chang'e (blue) and LGWA (orange). The results from a full integration of Eq. (9) are shown as the dashed horizontal lines. The approximate results calculated by Eq. (12) are plotted in solid lines.

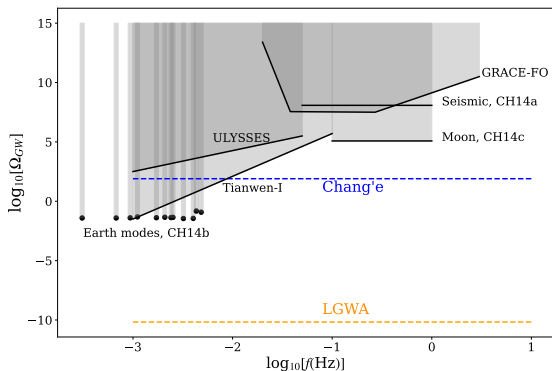


FIG. 4. Constraints on the SGWB given by Chang'e and LGWA (this work), as well as by ULYSSES [23], Earth's normal modes (CH14a), lunar seismic motion (CH14c), GRACE-FO [26], and Tianwen-I [27]. Following the style in [26], gray shaded area indicates the excluded region.

0.1Hz, the constraint given by Chang'e will be better than the previous ones by about two orders of magnitude. The constraint by LGWA will greatly exceed any current constraints in the frequency band of $10^{-3} - 1$ Hz, even though the threshold Ω_{GW} derived in this work is slightly worse than the previous prediction [28] because of the more up-to-date response functions used here.

V. SUMMARY AND DISCUSSIONS

Motivated by the recent improvements in the calculation of the response of the moon to GWs [31, 32, 34], we revisited in this paper the detectability of the SGWB by lunar seismometers. Besides applying the updated response functions, we paid special attention to the effect

imposed by the orientations of the seismometers, which are not necessarily pointing in a direction vertical to the moon surface due to different deployment mechanisms. To evaluate such an effect, we derived the pattern functions of a single seismometer for the two GW polarizations (Sec. II A). We note that these pattern functions will be useful for future studies of the localization of GW sources by lunar seismometer arrays.

Using the pattern functions, we also constructed the ORFs for a network of two seismometers (Sec. III A) as well as an array of an arbitrary number of seismometers (Sec. III B). We applied our ORFs to two future projects, namely, Chang'e and LGWA (Sec. IV). We found that in the frequency band around 0.1 Hz, the threshold SGWB detectable by Chang'e is two orders of magnitude better than the limit given previously by other missions. The sensitivity of LGWA would be even better, reaching a level as low as $\Omega_{\text{GW}}^{\text{LGWA}} \sim 6.7 \times 10^{-11}$ throughout the mid-frequency band of $10^{-3} - 10$ Hz (Fig. 4).

Finally, we point out several caveats in this work which deserve future investigation. First, we have omitted the correlation between the noise of the seismometers, which will be crucial for the seismometers placed at close locations. This correlation may undermine the ability of a seismometer array in constraining the SGWB. Second, as we have mentioned in Yan24, we ignored the complex structure at the surface of the moon. This structure might influence the lunar response functions [34], and should be examined by the real data from future lunar seismometers. Third, a recent theoretical study of the interaction between GW and elastic body hints that the current model of the lunar response may be incomplete [32]. The difference between the results deserves further investigation.

ACKNOWLEDGMENTS

This work is supported by the National Key Research and Development Program of China Grant No. 2021YFC2203002, the Beijing Natural Science Foundation No. 1242018, and the National Natural Science Foundation of China (NSFC) Grants No. 11991053, No. 12073005, No. 12021003, No. 42325406. The authors would like to thank Jan Harms for useful discussions and comments.

Appendix A: Proving that Eq. (4) applies to both polarizations

We first consider a new polarization state of GW that is different from Eq. (1). It can be written as

$$\mathbf{h}_{\text{new}} = \Re \left\{ h_0 \epsilon_{ij, \text{new}} e^{i(\omega_g t - \vec{k}_g \cdot \vec{r})} \right\}, \quad (\text{A1})$$

where

$$\epsilon_{ij,\text{new}} = \begin{bmatrix} 1 & -1 & 0 \\ -1 & -1 & 0 \\ 0 & 0 & 0 \end{bmatrix}. \quad (\text{A2})$$

To prove that this type of polarization also satisfies Eq. (4), the key step is to prove that it satisfies Eq. (25) in Yan24. The latter proof requires us to calculate the function f_{new}^m , which depends on the wave vector direction and polarization state (i.e., angles e, λ and ν in Ma19). Notice that in Ma19 and Yan24 the function f^m was calculated only for a specific polarization state.

Considering the definitions of angles e, λ and ν , we find that f_{new}^m can be obtained by replacing these angles with $(e + \pi), \lambda$, and $(\pi - \nu)$ respectively, which results in $\vec{l} \rightarrow \vec{l}, \vec{m} \rightarrow -\vec{m}$, and $\hat{e}_k \rightarrow -\hat{e}_k$. As a result, we get:

$$\begin{aligned} f_{\text{new}}^m &= f^m(e = \pi, \lambda = 0, \nu = \pi) \\ &= 4\sqrt{\frac{\pi}{15}} \times (-\delta_{m,2} + \delta_{m,-2}). \end{aligned} \quad (\text{A3})$$

Now we can combine the previously derived functions. On one hand, using the definitions of the three base vec-

tors, we can derive

$$\begin{aligned} \hat{e}_r \cdot \epsilon_{\text{new}} \cdot \hat{e}_r &= \sin^2 \theta (-\sin 2\varphi + \cos 2\varphi), \\ \hat{e}_\theta \cdot \epsilon_{\text{new}} \cdot \hat{e}_r &= \sin \theta \cos \theta (-\sin 2\varphi + \cos 2\varphi), \\ \hat{e}_\varphi \cdot \epsilon_{\text{new}} \cdot \hat{e}_r &= \sin \theta (-\sin 2\varphi - \cos 2\varphi). \end{aligned} \quad (\text{A4})$$

On the other hand, considering the definition of the real spherical harmonics and f_{new}^m , we have:

$$\begin{aligned} \sum_m \mathcal{Y}_{2m}(\theta, \varphi) f_{\text{new}}^m &= \sin^2 \theta (-\sin 2\varphi + \cos 2\varphi), \\ \sum_m \partial_\theta \mathcal{Y}_{2m}(\theta, \varphi) f_{\text{new}}^m &= \sin 2\theta (-\sin 2\varphi + \cos 2\varphi), \\ \sum_m \frac{\partial_\varphi \mathcal{Y}_{2m}(\theta, \varphi)}{\sin \theta} f_{\text{new}}^m &= 2 \sin \theta (-\sin 2\varphi - \cos 2\varphi). \end{aligned} \quad (\text{A5})$$

Therefore, we find

$$\begin{aligned} \frac{1}{2} \hat{e}_r \cdot \mathbf{h}_{\text{new}} \cdot \hat{e}_r &= \frac{h_0 \cos(\omega_g t)}{2} \sum_m \mathcal{Y}_{2m}(\theta, \varphi) f_{\text{new}}^m, \\ \frac{1}{2} \hat{e}_\theta \cdot \mathbf{h}_{\text{new}} \cdot \hat{e}_r &= \frac{h_0 \cos(\omega_g t)}{4} \sum_m \partial_\theta \mathcal{Y}_{2m}(\theta, \varphi) f_{\text{new}}^m, \\ \frac{1}{2} \hat{e}_\varphi \cdot \mathbf{h}_{\text{new}} \cdot \hat{e}_r &= \frac{h_0 \cos(\omega_g t)}{4} \sum_m \frac{\partial_\varphi \mathcal{Y}_{2m}(\theta, \varphi)}{\sin \theta} f_{\text{new}}^m. \end{aligned} \quad (\text{A6})$$

This concludes the proof that Eq. (25) in Yan24 is still satisfied when we consider a different polarization state.

-
- [1] J. Weber, Detection and Generation of Gravitational Waves, *Physical Review* **117**, 306 (1960).
- [2] J. Weber, Gravitational Waves, *Physics Today* **21**, 34 (1968).
- [3] T. S. Mast, J. E. Nelson, and J. A. Saarloos, Search for Gravitational Radiation from Pulsars, *Astrophysical Journal* **187**, L49 (1974).
- [4] C. W. Misner, K. S. Thorne, and J. A. Wheeler, *Gravitation* (W. H. Freeman and Company, San Francisco, 1973).
- [5] A. Ben-Menahem, Excitation of the earth's eigenvibrations by gravitational radiation from astrophysical sources., *Nuovo Cimento C Geophysics Space Physics C* **6**, 49 (1983).
- [6] A. Abramovici, W. E. Althouse, *et al.*, LIGO: The Laser Interferometer Gravitational-Wave Observatory, *Science* **256**, 325 (1992).
- [7] F. Acernese, M. Agathos, *et al.*, Advanced Virgo: a second-generation interferometric gravitational wave detector, *Classical and Quantum Gravity* **32**, 024001 (2015), arXiv:1408.3978 [gr-qc].
- [8] Kagra Collaboration, T. Akutsu, M. Ando, *et al.*, KAGRA: 2.5 generation interferometric gravitational wave detector, *Nature Astronomy* **3**, 35 (2019), arXiv:1811.08079 [gr-qc].
- [9] M. Colpi, K. Danzmann, *et al.*, LISA Definition Study Report, arXiv e-prints, arXiv:2402.07571 (2024), arXiv:2402.07571 [astro-ph.CO].
- [10] J. Luo, L.-S. Chen, H.-Z. Duan, *et al.*, TianQin: a spaceborne gravitational wave detector, *Classical and Quantum Gravity* **33**, 035010 (2016), arXiv:1512.02076 [astro-ph.IM].
- [11] Z. Luo, Y. Wang, Y. Wu, W. Hu, and G. Jin, The Taiji program: A concise overview, *Progress of Theoretical and Experimental Physics* **2021**, 05A108 (2021).
- [12] M. Arca Sedda, C. P. L. Berry, K. Jani, *et al.*, The missing link in gravitational-wave astronomy: discoveries waiting in the decihertz range, *Classical and Quantum Gravity* **37**, 215011 (2020), arXiv:1908.11375 [gr-qc].
- [13] B. Allen and J. D. Romano, Detecting a stochastic background of gravitational radiation: Signal processing strategies and sensitivities, *Phys. Rev. D* **59**, 102001 (1999), arXiv:gr-qc/9710117 [gr-qc].
- [14] B. Allen, Stochastic gravity-wave background in inflationary-universe models, *Phys. Rev. D* **37**, 2078 (1988).
- [15] R. Easther and E. A. Lim, Stochastic gravitational wave production after inflation, *Journal of Cosmology and Astroparticle Physics* **2006** (4), 010, arXiv:astro-ph/0601617 [astro-ph].
- [16] C. Caprini and D. G. Figueroa, Cosmological backgrounds of gravitational waves, *Classical and Quantum Gravity* **35**, 163001 (2018), arXiv:1801.04268 [astro-ph.CO].

- [17] A. J. Farmer and E. S. Phinney, The gravitational wave background from cosmological compact binaries, *Monthly Notices of the Royal Astronomical Society* **346**, 1197 (2003), arXiv:astro-ph/0304393 [astro-ph].
- [18] P. A. Rosado, Gravitational wave background from binary systems, *Phys. Rev. D* **84**, 084004 (2011), arXiv:1106.5795 [gr-qc].
- [19] N. Karnesis, S. Babak, M. Pieroni, N. Cornish, and T. Littenberg, Characterization of the stochastic signal originating from compact binary populations as measured by LISA, *Phys. Rev. D* **104**, 043019 (2021), arXiv:2103.14598 [astro-ph.IM].
- [20] M. Coughlin and J. Harms, Upper Limit on a Stochastic Background of Gravitational Waves from Seismic Measurements in the Range 0.05-1 Hz, *Phys. Rev. Lett.* **112**, 101102 (2014), arXiv:1401.3028 [gr-qc].
- [21] M. Coughlin and J. Harms, Constraining the gravitational wave energy density of the Universe using Earth's ring, *Phys. Rev. D* **90**, 042005 (2014), arXiv:1406.1147 [gr-qc].
- [22] M. Coughlin and J. Harms, Constraining the gravitational-wave energy density of the Universe in the range 0.1 Hz to 1 Hz using the Apollo Seismic Array, *Phys. Rev. D* **90**, 102001 (2014), arXiv:1409.4680 [gr-qc].
- [23] B. Bertotti, R. Ambrosini, J. W. Armstrong, S. W. Asmar, G. Comoretto, G. Giampieri, L. Iess, Y. Koyama, A. Messeri, A. Vecchio, and H. D. Wahlquist, Search for gravitational wave trains with the spacecraft ULYSSES., *Astronomy and Astrophysics* **296**, 13 (1995).
- [24] A. S. Konopliv, S. W. Asmar, E. Carranza, W. L. Sjogren, and D. N. Yuan, Recent Gravity Models as a Result of the Lunar Prospector Mission, *Icarus* **150**, 1 (2001).
- [25] S. Aoyama, Upper limit on the amplitude of gravitational waves around 0.1Hz from the Global Positioning System, in *Quest for the Origin of Particles and the Universe*, edited by Y. Aoki and et al. (2013) p. 29.
- [26] M. P. Ross, C. A. Hagedorn, E. A. Shaw, A. L. Lockwood, B. M. Iritani, J. G. Lee, K. Venkateswara, and J. H. Gundlach, Limits on the stochastic gravitational wave background and prospects for single-source detection with GRACE Follow-On, *Phys. Rev. D* **101**, 102004 (2020), arXiv:2002.02044 [gr-qc].
- [27] X. Bi, Z. Guo, X. Zou, Y. Huang, P. Li, J. Cao, L. Chen, W. Tang, and Y. Kau Lau, Doppler Tracking Data of Martian Mission Tianwen-I and Upper Limit of Stochastic Gravitational Wave Background, arXiv e-prints , arXiv:2402.06096 (2024), arXiv:2402.06096 [gr-qc].
- [28] J. Harms, F. Ambrosino, L. Angelini, *et al.*, Lunar Gravitational-wave Antenna, *Astrophys. J.* **910**, 1 (2021), arXiv:2010.13726 [gr-qc].
- [29] J. Li, F. Liu, Y. Pan, Z. Wang, M. Cao, M. Wang, F. Zhang, J. Zhang, and Z.-H. Zhu, Detecting gravitational wave with an interferometric seismometer array on lunar nearside, *Science China Physics, Mechanics, and Astronomy* **66**, 109513 (2023).
- [30] J. Majstorović, S. Rosat, and Y. Rogister, Earth's spheroidal motion induced by a gravitational wave in flat spacetime, *Phys. Rev. D* **100**, 044048 (2019).
- [31] H. Yan, X. Chen, J. Zhang, F. Zhang, M. Wang, and L. Shao, Toward a consistent calculation of the lunar response to gravitational waves, *Phys. Rev. D* **109**, 064092 (2024).
- [32] E. Belgacem, M. Maggiore, and T. Moreau, Coupling elastic media to gravitational waves: an effective field theory approach, arXiv e-prints , arXiv:2403.16550 (2024), arXiv:2403.16550 [gr-qc].
- [33] M. Kachelriess and M. P. Nødtvedt, Lunar response to gravitational waves, arXiv e-prints , arXiv:2312.11665 (2023), arXiv:2312.11665 [gr-qc].
- [34] X. Bi and J. Harms, The response of the Moon to gravitational waves, arXiv e-prints , arXiv:2403.05118 (2024), arXiv:2403.05118 [gr-qc].
- [35] C. Li, C. Wang, Y. Wei, and Y. Lin, China's present and future lunar exploration program, *Science* **365**, 238 (2019).
- [36] Y. Zou, Y. Liu, and Y. Jia, Overview of China's Upcoming Chang'E Series and the Scientific Objectives and Payloads for Chang'E 7 Mission, in *51st Annual Lunar and Planetary Science Conference*, Lunar and Planetary Science Conference (2020) p. 1755.
- [37] C. Wang, Y. Jia, *et al.*, Scientific objectives and payload configuration of the Chang'E-7 mission, *National Science Review* **11**, nwad329 (2023), <https://academic.oup.com/nsr/article-pdf/11/2/nwad329/56730230/nwad329.pdf>.
- [38] M. P. Panning, S. Kedar, *et al.*, Farside Seismic Suite: Update on the Status of the First Seismic Station on the Farside of the Moon, in *LPI Contributions*, LPI Contributions, Vol. 3040 (2024) p. 2354.
- [39] N. J. Kanu, E. Gupta, and G. C. Verma, An insight into India's Moon mission - Chandrayan-3: The first nation to land on the southernmost polar region of the Moon, *Planetary and Space Science* **242**, 105864 (2024).
- [40] M. Maggiore, Gravitational waves. Volume 1: theory and experiments. Oxford University Press, 2007, 576p., GBP47.00, ISBN13: 978-0-19-857074-5, *General Relativity and Gravitation* **41**, 1667 (2009).
- [41] Chang'e 7 and 8 landers will both land near the lunar south pole.
- [42] J. V. van Heijningen, H. J. M. ter Brake, *et al.*, The payload of the Lunar Gravitational-wave Antenna, *Journal of Applied Physics* **133**, 244501 (2023), arXiv:2301.13685 [gr-qc].
- [43] P. Lognonné, W. B. Banerdt, D. Giardini, *et al.*, SEIS: Insight's Seismic Experiment for Internal Structure of Mars, *Space Science Reviews* **215**, 12 (2019).